June 23, 1998

A Test for Coronal Magnetic Field Extrapolations

Jeongwoo Lee, Stephen M. White, Mukul R. Kundu
Astronomy Department, University of Maryland, College Park, MD 20742

Zoran Mikić
Science Applications International Corporation, San Diego, CA 92121

and

A. N. McClymont
Institute for Astronomy, University of Hawaii, Honolulu, HI 96822

ABSTRACT

As models for the physical properties of the corona above solar active regions grow more sophisticated, we will require better means for testing them. In this paper we discuss and apply such a test to a magnetic field model for an active region. This test is based on the expectation that the temperatures at different points on a given magnetic field line should be well correlated, due to the rapid transport of heat along field lines in the corona. We use radio observations of an active region to measure the temperatures on field lines as they cross two isogauss surfaces (at 430 and 750 G) in the corona. The field lines and isogauss surfaces are derived from a coronal magnetic field model obtained via a nonlinear force–free field extrapolation of a photospheric vector magnetogram; for comparison, we also investigate a potential–field extrapolation of the same magnetogram. In a region where strongly sheared fields are present, the nonlinear force–free field model does indeed show a good correlation between the temperatures in the two surfaces at points on the same field line, while the potential–field model does not. This diagnostic acts both as a test of the magnetic field model as well as of the interpretation of the radio data, and we show how this test can also aid in understanding the radio data.

Subject headings: Sun: corona — Sun: magnetic fields — Sun: radio radiation

1. Introduction

The determination of the magnetic field structure of the solar corona is a goal being pursued by a number of complementary techniques. The ability to measure this quantity is widely regarded as an important stepping stone in the path to understanding many of the major unsolved problems of solar physics. Three main techniques contribute to this effort: optical observations of vector magnetic fields in the photosphere and their extrapolation into the corona; EUV/X–ray observations which can reveal the projected paths of magnetic field lines via the density contrast between neighbouring bundles of field lines; and radio observations which are sensitive to both the strength and direction of the coronal magnetic field. The three techniques each have their own advantages and disadvantages, and we are presently still very much in the phase of learning how best to use them (e.g., McClymont, Jiao & Mikić 1997; Bastian, Gary, & White 1998). It is clear that the strengths of each technique will have to be combined with those of the others in order to make progress. In particular, the success of extrapolation of photospheric field measurements into the corona needs to be tested against coronal observations. One such test is the comparison of field line trajectories predicted by the field extrapolations with coronal X–ray images which delineate that subset of field lines which carry high densities (e.g., Jiao, McClymont, & Mikić 1997).

Radio data may also be used as a diagnostic of coronal magnetic structure. The property which makes this possible is the fact that solar active regions of high magnetic field strength are generally optically thick due to gyroresonant opacity at frequencies above $\sim$ 3 GHz (e.g., White & Kundu 1997). Being a resonant mechanism, gyroresonance provides a known relationship between a specific microwave frequency, f, and the coronal magnetic field strength, B, in the optically thick layer: $f = 2.8 \times 10^6\, n\, B$, with f in MHz and B in gauss and where n (the harmonic number) is an integer usually taking the value 2, 3 or 4 (Zheleznyakov 1962, Zlotnik 1968a,b). Therefore observing gyroresonant emission at some frequency indicates the presence of a particular field strength somewhere in the corona along the line of sight, as long as the appropriate harmonic number is known (e.g., Hurford & Gary 1986, Holman 1992, Gary & Hurford 1994). Only the highest optically thick harmonic layer in the atmosphere is relevant since all lower–lying layers (corresponding to higher B and hence smaller n) are obscured. Traditionally radio observers have used plasma parameters derived from observations at soft X ray and EUV wavelengths to determine the the highest value of n which is optically thick (the effective harmonic). In practice the field orientation and magnetic scale length are needed for this calculation as well as the plasma parameters (Schmelz et al. 1995, 1992; Brosius et al. 1992; Nitta et al. 1991). Alternatively the harmonic could be determined with use of magnetic flux conservation (Lee, Hurford, & Gary 1993) or the stereoscopic method (Aschwanden et al. 1995).

Since the resulting coronal field strength is a measured value, it may be compared with theoretical magnetic field models. For instance, Schmelz et al. (1992, 1995) and Brosius et al. (1997) compared their field measurements with potential (current-free) field extrapolations to test the validity of the potential field assumption for the active regions of interest. In other cases, results from radio observations of simple sunspots have been compared with analytical models to address the force balance of sunspot fields at coronal heights (Vourlidas, Bastian, & Aschwanden 1997, Lee et al. 1993). However, a problem with these approaches is that the height of the optically thick radio source is not measurable from a single observation so that the appropriate model height for comparison is not known, and coronal magnetic fields decrease so rapidly with height that this renders comparison difficult. Another problem was noted by Schmelz et al. (1992, 1995): coronal field strengths predicted by extrapolation of photospheric fields are very sensitive to errors (such as saturation) and uncertainty in the photospheric magnetic field measurements. Therefore in cases where strong field strengths derived from radio observations exceed those predicted by potential field extrapolations there is always some uncertainty as to whether the cause is the presence of nonpotential fields or errors in the photospheric magnetograms (Lee et al. 1997, Alissandrakis, Kundu, & Lantos 1980).

There is another class of radio studies which address the field-line connectivity as well as field strength, and its relationship to temperature structure in the corona. Schmahl et al. (1982), Alissandrakis & Kundu (1984), and Nindos et al. (1996) compared their observations with calculations of radio emission using magnetic field models calculated using linear force-free field extrapolations (i.e., the field is assumed to obey $\nabla \times \mathbf{B} = \alpha\mathbf{B}$ where α is a constant) to find that morphology of the gyroemission itself strongly limits the possible choice of α. Chiuderi-Drago, Alissandrakis, & Hagyard (1987) carried out detailed modelling of coronal temperature structure along individual field lines in the context of two–dipole models for the coronal magnetic field. Klimchuk & Gary (1995) also used a field–line–structured plasma model to interpret the difference between soft X–ray and radio observations. Lee et al. (1998a) calculated gyroresonant emission from field–line–structured temperature models using a magnetic field model calculated via a nonlinear force-free field extrapolation of photospheric vector magnetograms to demonstrate that both the magnetic field models and field–line structured temperature models can be tested against radio images self-consistently. Field–line approaches such as these have the advantage that they are less sensitive to errors in the magnetogram than are predictions of the field strength.

In this paper, we present a new use of multi–frequency radio observations to test the field-line connectivity predicted by a field extrapolation. We exploit a unique property of gyroresonant radiation: because it is a resonant mechanism and optically thick, emission arises on a relatively thin (typically 100 km in depth) surface of constant magnetic field strength. The measured temperatures are characteristic of very localized regions on this surface, unlike temperatures determined from optically thin emissions such as EUV lines which are emission–measure–weighted averages of all the material in a resolution element along the line of sight. We combine this property of the radio emission with improved coronal magnetic field models made feasible by recent progress in coronal field extrapolation. It is now possible to calculate nonlinear (non-constant-α) force-free fields in the corona, given photospheric vector magnetogram measurements (McClymont, Jiao, & Mikić 1997). Favorable comparisons with observations of the thickness of coronal loops (McClymont & Mikić 1994), SXT X-ray loops (Jiao, McClymont, & Mikić 1997), Hα emission during a flare (Mikić & McClymont 1994), and radio observations (Lee et al. 1998a,b) indicate that coronal magnetic fields estimated in this fashion are reasonably accurate.

Our idea is as follows: at any one frequency, the radio emission represents a true local coronal electron temperature on a thin isogauss surface (as long as it is dominated by optically thick gyroresonance emission). By varying the frequency of observation, different gyroresonant surfaces, and therefore different layers of the corona, are sampled. Two such layers at different frequencies will generally be connected by magnetic field lines common to both. Because cross–field transport of physical quantities is so much weaker than field–aligned transport in a plasma such as the solar corona, there are strong theoretical reasons for expecting that the temperatures at points connected by the same field line should be well correlated. The observation that the corona at X–ray wavelengths is dominated by filamentary structure as expected from a field–line structured corona (e.g., Golub 1996) is strong evidence in favor of this idea. The temperature will not necessarily be the same everywhere on a field line, although theory on coronal loops indicates that the coronal temperature is nearly uniform along a field line over much of the loop around the apex (Rosner, Tucker, & Vaiana 1978, Craig, McClymont, & Underwood 1978, Vesecky, Antiochos, & Underwood 1979, Jordan 1980, Serio et al. 1981, Pallavicini et al. 1981, Klimchuk, Antiochos, & Mariska 1987). High resolution EUV observations supporting such theoretical ideas on field–line–structured coronal temperatures are now available (Kankelborg et al. 1996, Neupert et al. 1997). However, whatever the actual dependence, we expect that different points on a field line should "know" about the temperature elsewhere on the field line and show a correlation. This suggests the following test: if we have radio images at several frequencies which represent local electron temperatures on different isogauss surfaces in the corona, then the temperatures at points connected by field lines should show a good correlation. If either the field line model fails to accurately represent the connectivity, or if there are problems with the radio data (such as non–uniqueness in the deconvolution problems or because the wrong harmonic has been calculated), we do not expect any significant correlation. We carry out such a test in this paper.

2. The Proposed Test of Field Extrapolations

2.1. Data and Field Extrapolations

We use radio and magnetic data for AR 6615 on 1991 May 7 as an example to illustrate and apply our test. AR 6615 is a complex active region possessing strong currents. The radio data consist of excellent images at 4.9 (resolution $8''$) and 8.4 GHz (resolution $5''$) in both right and left circular polarizations made using the VLA[1] on 1991 May 7. The data analysis is described in Lee et al. (1997).

We obtain the coronal magnetic field model by extrapolating the photospheric fields into the corona using a vector magnetogram obtained from the Haleakala Stokes polarimeter at Mees Solar Observatory at 17:20 UT (Fig. 2 of Lee et al. 1998a) as the boundary condition. The nonlinear force–free magnetic field extrapolation (FFF), including the role of non–potential fields, is performed using the evolutionary method (Mikić and McClymont, 1994), allowing a long enough evolution time to assure full relaxation of the magnetic field lines. Possible uncertainties in the boundary condition and advantages of this method of field extrapolation over other types of extrapolations have been discussed by McClymont, Jiao, & Mikić (1997). Here we address the validity of the field–line connectivity found in this extrapolation with the test described above. For comparison purposes, we also investigate the connectivity in a potential field (PF) model which ignores currents and which has already been found to predict inadequate coronal magnetic field strengths (Lee et al., 1997).

2.2. Basic Idea

For the purpose of illustrating the proposed method, we plot in Figure 1 the observed intensity distributions at 4.9 GHz and 8.4 GHz on two hypothetical, simplified emission layers (simplified in the sense that the true isogauss surfaces are not flat as represented in this figure). As long as the emission is dominated by optically thick gyroresonance emission, the emission layer is a thin isogauss surface and microwave images in the sky plane (x, y) at

[1]The VLA is operated by the National Radio Astronomy Observatory, which is a facility of the National Science Foundation operated under cooperative agreement by Associated Universities, Inc.

two different frequencies represent electron temperatures in two isogauss surfaces separated from each other along the line of sight, z. Our procedure is to start at a point in one of the emission layers (e.g., the 4.9 GHz emission layer) and to trace the field line passing through this point until it intersects the other (8.4 GHz) layer, if it does so; if it does not (i.e., it never passes through a region of sufficient field strength), we ignore it. The brightness temperatures in each layer at points connected by a field line are read from the images. As long as the coronal temperature distribution is structured along field lines we expect a good correlation between the temperatures in the two layers connected by a common field line: i.e., we expect that hot regions in both emission layers are connected by field lines such as those numbered 1 and 3 in Figure 1, while cool regions are connected by field lines such as line 2. There can also be field lines such as line 4 which intersect only one emission layer (the 8.4 GHz emission layer in this case, because the minimum field strength found on this field line is too high to pass through the other layer). Such field lines (while useful for understanding why images can look so different at different frequencies) cannot be used for our purposes and will be excluded.

2.3. A Preliminary Check

Although this comparison sounds simple on the face of it, there are a couple of effects of which we must be careful. One important complication is the need to identify the appropriate effective harmonic (the highest optically thick harmonic) n for each radio image. In the solar corona the two natural propagating electromagnetic modes are circularly polarized nearly everywhere except where the direction of propagation is orthogonal to the local magnetic field. One mode (the X mode) gyrates in the same sense as an electron about the magnetic field and interacts more strongly with the plasma than the other mode (the O mode, which gyrates in the opposite sense). The two natural modes are observed by the VLA as opposite circular polarizations. The effective harmonic is in general different for the two polarizations and may vary from place to place for a given polarization due to changes in the plasma parameters and in the inclination between the magnetic field and the line of sight across the isogauss layer (e.g., Zlotnik 1968a,b, White & Kundu 1997). We will calculate the effective harmonic as a function of position at each observing frequency using the magnetic field model and local plasma parameters on the gyroresonant surfaces rather than using quantities averaged along the line-of-sight.

For this purpose, we use the observed radio temperatures as trial values for the electron temperature on the relevant harmonic layers. For instance, we proceed to calculate the opacity at the fourth harmonic at 4.9 GHz using the observed brightness temperature at

4.9 GHz as the electron temperature on the harmonic layer. If the resulting opacity is too small to make the $n = 4$ layer optically thick then our assumption on the effective harmonic is self-contradictory. However, if the opacity is found to be greater than unity, the effective harmonic we assumed is, at least, possible. All the magnetic quantities needed for the calculation of gyroresonant opacity, such as magnetic field inclination angle and magnetic scale height, have been calculated on all possible harmonic layers (see Fig. 4 of Lee et al. 1998a). By field line tracing, we are also able to calculate the lengths of the field lines passing through the harmonic layers, which are used together with the temperatures assumed per field line in the well-known scaling law for quasistatic loops of Rosner, Tucker, and Vaiana (1978) to derive densities of individual field lines. Note that the density derived from the scaling law is actually appropriate at the loop apex and may be a slight underestimate of the density in a gyroresonant layer below the loop top. These densities, temperatures, and magnetic quantities evaluated on the harmonic layers of concern are used to calculate theoretical gyroresonant opacities at the two observing frequencies and at both X and O modes.

Figure 2 shows the results. The contours show the levels of $\tau_n = 1$ for either $n = 3$ or $n = 4$, with the interior of the contour being optically thick. We identify the left and right circularly (LC and RC, respectively) polarized waves with the X and O modes, respectively, in the northern half of the active region where the photospheric longitudinal magnetic polarity is negative. In the southern half of the active region, the magnetic polarity is positive and the reverse is true; however, due to the presence of a quasi-transverse layer overlying the southern region, the modes are reversed while propagating away from the Sun and the LC polarized waves are again the X mode, and the right, the O modes (see Lee et al. 1998b, for details). Hereafter, we denote the brightness temperatures in the LC and RC polarization states as T_X and T_O, respectively. Since the X mode is always more likely to be optically thick than the O mode, we use T_X as electron temperature, T_e, in calculation of the opacity. Figure 2 shows that the brightest radio emission regions are optically thick up to the fourth harmonic for all frequencies and both polarizations, with the exception of the O mode at 8.4 GHz.

3. Results

Like most other active regions, magnetic shear in this active region is also localized. The magnetic fields produced by the FFF extrapolation are largely different from the potential fields in the regions where strong magnetic shear is present and this is the place we want to test the FFF extrapolation. But in regions where shear is weak, the distinction between the PF and the FFF model tends to vanish and we should be able to see a good correlation of temperatures on the two radio emission layers connected by the field lines regardless of the extrapolation. We thus apply this test first to a potential-like region in Figure 3, and next to the strongly sheared region in Figure 4 and 5. In all figures hereafter we present T_X and T_O in units of 10^6 K.

In Figure 3 we apply the test to a potential-like region which lies in the eastern part of the active region (the region around the field line 1 in Figure 1, see Lee et al. 1998 for distribution of currents). Assuming $n = 4$ means that the 4.9 and 8.4 GHz emission layers are the surfaces of constant magnetic field in the corona at field strengths of 430 G and 750 G, respectively. We perform field line tracing from the 430 G isogauss surface to the 750 G isogauss surfaces and determine the brightness temperatures at each surface for both polarizations. In each case, the connected points are shown in the left panels, which display the 8.4 GHz emission as a grey–scale image with the 4.9 GHz emission overplotted as black contours. The starting points on the 4.9 GHz surface are shown as black crosses and form a regular rectangular grid of spacing $2''$ (compared to the restoring beam size of $5''$ at 8.4 GHz) in projection, while the corresponding points on the 8.4 GHz surface connected by field lines (or line of sight) to the 4.9 GHz points are shown as white symbols. The white plus symbols right underneath the black plus symbols indicate those points connected by the line of sight; the white plus and diamond symbols are those connected by potential field lines and nonlinear force–free field lines, respectively. As expected, the PF and the FFF extrapolation predict the field lines with only a little difference in this potential-like region. To the right of each image, the corresponding scatter plot of brightness temperature at 4.9 GHz versus that at 8.4 GHz for the connected points is shown together with linear correlation, r. Both the PF and the FFF extrapolations predict equally an excellent temperature correlation for X mode ($r > 0.9$) and a moderately good correlation for O mode ($r \approx 0.6$). On the other hand, the temperatures on the two radio emission layers connected by the line of sight show negative correlations for both modes. All these results support the idea of the field-line structured coronal temperature that we are assuming, and convince us that the proposed test for field line extrapolation works well.

We now go on to the region in which strong magnetic shear is present in order to see if the FFF still yields a good correlation whereas the PF fails to do. The strongest shear is found in the north-western part of the active region (the region around field line 3 in Figure 1) which also happens to be the location of the highest electron temperatures in the radio images (see Lee et al. 1997, 1998a). In Figure 4, we present the results of comparing the brightness temperatures for the X mode. Here three different correlations are shown for comparison: the 4.9 and 8.4 GHz temperatures on the points in the two layers connected by the line of sight only (top), temperatures at points connected by field lines in the PF model (middle), and points connected by field lines in the FFF model (bottom). While the line–of–sight connection shows no correlation ($r = 0.09$) and the potential–field model results in a negative correlation ($r = -0.18$), the field lines from the FFF model result in points which show a very good correlation ($r = 0.66$) between the two layers. The PF model predicts quite the wrong behaviour for the field lines in this region, moving too far to the south as they drop in height from the 4.9 GHz layer to the 8.4 GHz layer. In the FFF model the field lines move more to the west in projection as they drop in height.

In Figure 5 we repeat the same procedure using O mode images and connected points on the 430 and 750 G isogauss surfaces. There is considerably more uncertainty about the effective harmonic for the O mode, and in particular it is expected to vary with location in the image far more than for the X mode due to its stronger dependence on the inclination angle between the magnetic field and the line of sight. Indeed, in contrast to the situation for the X mode, in the O mode the brightness temperatures at the two frequencies do not correlate well in any of the models with the assumption that the emission arises on the $n = 4$ harmonic layers, although the FFF model does show more correlation than the line–of–sight or potential–field connections.

The 4.9 GHz O mode brightness temperatures generally exceed those at 8.4 GHz. A likely explanation for this is that the assumption that the $n = 4$ harmonic layer is optically thick is incorrect for the O mode: it has lower opacity than the X mode and, except for a narrow range of propagation angles nearly perpendicular to the local magnetic field direction, it is generally thought to be optically thick at a harmonic one lower than that which is optically thick in the X mode as Figure 2 suggests. Since the 8.4 GHz temperatures are below the 4.9 GHz temperatures, we investigate the possibility that 8.4 GHz may be optically thin in the $n = 4$ layer but optically thick in the lower $n = 3$ layer, while 4.9 GHz remains optically thick in the $n = 4$ layer. We therefore plot in the lower right panel of Figure 5 the points which result from the assumption that 8.4 GHz emission is optically thick in the 1000 G layer rather than the 750 G layer, using both the PF (crosses) and FFF (solid diamonds) models. The lower left panel of Figure 5 shows the positions of the corresponding points (black plus symbols for 4.9 GHz, white crosses for 8.4 GHz points in the PF model, and white squares for the 8.4 GHz points in the FFF model). Due to the larger shear in the field lines in the FFF model, the 8.4 GHz points are displaced further eastward from the 4.9 GHz connections than in the PF model. Many of the 8.4 GHz points now acquire higher temperatures at the new positions for the FFF model, and there are many more points than before for which $T_O^{4.9\mathrm{GHz}} \approx T_O^{8.4\mathrm{GHz}}$. It therefore seems likely that differing harmonics at different frequencies for different polarizations can partly explain the poor correlation of O mode temperatures shown in Figure 5. On the other hand, the PF model does not significantly improve with this change in assumed harmonic number, thus again indicating that the PF is inappropriate to describe magnetic fields in this region.

However, formally the linear correlation coefficient for the FFF model is actually now worse since the points are more spread out. There remain many points which do not show the behaviour ($T_O^{4.9\mathrm{GHz}} = T_O^{8.4\mathrm{GHz}}$) expected from loop models, even after the harmonic is adjusted. From inspection of the images in Figure 5, the correlation can only be improved if the points at the peak of the 4.9 GHz image connect to the peak in the 8.4 GHz image well to the north–east. It is unlikely that a better correlation can be achieved by trying other combinations of single harmonics at the two frequencies. Since the O mode opacity never exceeds the X mode opacity, the observation that $n = 4$ is correct for the X mode means that only lower harmonics can be optically thick in the O mode. If we assume $n = 3$ to be the effective harmonic for both the 4.9 GHz and 8.4 GHz emission, then both the emission surfaces are lower in the corona: the field lines will start from lower heights than in Figure 5, and the corresponding points in the $n = 3$ layer for 8.4 GHz will not be as far east as in Figure 5, making the temperature correlation worse. Assuming combinations of even lower harmonics makes the height difference between the two emission layers small, in which case the correlation is likely to be similar to that seen in the line–of–sight connections.

In addition to uncertainty in the harmonic, other factors may play a role in the observed scatter for the O mode. It may be partially optically thick at one harmonic, in which case the observed brightness temperature is actually a combination of temperatures in two adjacent harmonic layers. Due to the different opacities in the X and O modes, it is possible for this effect to be important in one mode but not the other. It is true that the highest optically thick harmonic can vary as the inclination angle (the angle between **B** and the line of sight) varies, and that this variation can occur more rapidly in the O mode than in the X mode for small viewing angles. However the field lines in the region under investigation have mostly large viewing angles. Another possible complication is real variation of temperature along some field lines. At the low effective harmonic for the O mode, $n = 3$, the emission requires 1000 G field strengths and much of the 8.4 GHz emission is located close to the footpoints of field lines. The expectation that temperature is nearly constant along a field line is only likely to be satisfied away from the footpoints (Rosner, Tucker, & Vaiana, 1978, Craig, McClymont, & Underwood 1978, Klimchuk, Antiochos, & Mariska 1987, Kankelborg et al. 1996), and thus may not be a good assumption for the O mode data.

4. Conclusion

Inferring the three–dimensional magnetic structure of the corona above solar active regions using the two–dimensional projections available in magnetic, EUV/X–ray or radio images is a difficult task. In this paper we have proposed and carried out an obvious test for such models by combining magnetic field and radio data. The diagnostic is made possible by two properties of microwave emission: it becomes optically thick in very narrow layers in the solar corona and therefore directly senses the local electron temperature in those layers; and by varying the frequency the radio images show different layers, so that frequency may be regarded as a height variable. The test is a relatively simple consequence of the well-known physics that the temperature distribution in the corona should be structured along field lines due to the anisotropy in transport properties along and across field lines in a strongly magnetized plasma such as the corona. Therefore, the temperature at different points on the same field lines should be well correlated, and the radio data can be used to measure the temperatures at points where a given field line crosses isogauss surfaces in which radio emission originates. The third dimension in this technique is therefore provided by frequency.

The main technique in which one attempts to reconstruct the third dimension has been rotational stereography (Aschwanden et al. 1995, Aschwanden, Bastian, & White 1992), where one assumes that an optically thin source remains unchanging while the Sun rotates and provides terrestrial observers with different perspectives from which all three dimensions may be reconstructed. Another technique has been employed by Brosius et al. (1997): the column emission measure and density derived from EUV emission line intensities are used in conjunction with radio images to determine magnetic field strength as a function of temperature, and the height of the coronal gyroresonant layers is then estimated from the thickness of the EUV emitting volumes assuming a filling factor. All these methods are complementary in the sense that stereoscopy using EUV/soft X–rays or radio bremsstrahlung favors higher density regions, while the microwave test operates only in regions of high coronal magnetic field strength. In addition, the latter two methods attempt to reconstruct the field strength distribution in the corona, whereas our method tests magnetic field lines predicted by field extrapolations.

The test used here can be expected to show a good correlation to the extent that the magnetic field line model represents the coronal field, and to the extent that the radio data are optically thick and can be correctly associated with particular isogauss surfaces. In general one cannot always be sure which harmonic surface n is the appropriate one to use, and the optically thick assumption may break down in regions where the temperatures are of order 10^6 K and below. For this reason we have focussed here on a region of high brightness temperature where we are confident that the radio data are optically thick. For the X mode, where the opacity varies less with inclination angle and a larger area of the corona should be optically thick at the same harmonic, we see a good correlation between the 4.9 GHz and 8.4 GHz brightness temperatures at points connected by field lines in the FFF model for $n = 4$, while the same test for a potential field model of the magnetic field clearly fails. As discussed above, there is still room for uncertainty in the appropriate harmonic to use for the O mode data, but by adjusting the harmonics used we can improve the correlation to some extent. In this way the test acts both to test the magnetic field model as well as the interpretation of the radio data. The test is also limited here by the resolution of both the radio and magnetic data, and higher resolution would be desirable to provide more stringent tests.

The test carried out here requires radio data which give confidence in predicting the dominant radiation mechanism and the extrapolated magnetic field lines. This active region (AR 6615) was particularly well suited to this test because it was optically thick at microwave wavelengths over a large area of the corona, and because it contained strong nonpotential fields. Clearly, the success of the test in this single instance is not proof that extrapolation techniques are now completely reliable: the good correlation obtained here needs to be replicated with other data before we can declare this technique a success, and the difficulties with the O mode need to be resolved. However, if it proves to be valid then various extensions of the present diagnostic should be possible in future studies. For instance, it may help to resolve the 180° ambiguity in vector magnetograms by looking at which assumption for the azimuthal angle yields extrapolated field lines in best agreement with multiwavelength microwave images. Having convinced ourselves of the field line connectivity through this test, we can further investigate possible correlations between the temperature of a loop and its magnetic parameters. Such studies have previously been carried out using soft X–ray and EUV images (e.g., Jiao, McClymont, & Mikić 1997). The unique property of microwave data in being optically thick in narrow layers and thus sensing local temperatures lends itself to coronal temperature studies, and in particular we hope to address the issue of the spread of temperatures inferred from EUV spectra of active regions.

We thank the anonymous referee for his careful review and many helpful suggestions. This work has been supported by NSF grant ATM-96-12738 and NASA grant NAG-W-1541. Z. M. has been supported by NASA contract NASW-4728 and NSF grant ATM-9320575. A. N. M. has been supported by ATM 93-20575 and ATM 96-13794.

REFERENCES

Alissandrakis, C. E. & Kundu, M. R. 1984, A&A, 139, 271

Alissandrakis, C. E., Kundu, M. R., & Lantos, P. 1980, A&A, 82, 30.

Aschwanden, M. J., Bastian, T. S., & White, S. M. 1992, in ESA, Proceedings of the First SOHO Workshop: Coronal Streamers, Coronal Loops, and Coronal and Solar Wind Composition, p 217

Aschwanden, M. J., Lim, J., Gary, D. E., & Klimchuk, J. A. 1995, ApJ, 454, 512

Bastian, T. S., Gary, D. E., & White, S. M.: 1998, in Synoptic Solar Physics, eds. K. S. Balasubramaniam, J. W. Harvey and D. M. Rabin, Astron. Soc. Pacific (San Francisco), in press

Brosius, J. W., Wilson, R. F., Holman, G. D., & Schmelz, J. T. 1992, ApJ, 386, 347

Brosius, J. W., Davila, J. M., Thomas, R. J., & S. M. White 1997, ApJ, 488, 488

Chiuderi-Drago, F., Alissandrakis, C.,& Hagyard, M. 1987, Sol. Phys., 112, 89

Craig, I. J. D., McClymont, A. N., & Underwood, J. H. 1978, A&A, 70, 1

Gary, D. E. & Hurford, G. J. 1994, ApJ, 420, 903

Golub, L. 1996, Ap&SS, 237, 33.

Holman, G. D. 1992, in ESA, Proceedings of the First SOHO Workshop: Coronal Streamers, Coronal Loops, and Coronal and Solar Wind Composition, p. 189

Hurford, G. J. & Gary, D. E. 1986, Coronal Processes and Plasmas, NASA Conference Proc. 2442

Jiao, L., McClymont, A. N., & Mikić, Z. 1997, Sol. Phys., 174, 311

Jordan, C. 1980, A&A, 86, 355

Kankelborg, C. C., Walker A. B. C., Hoover, R. B., & Barbee, T. R., Jr. 1996, ApJ, 466, 529

Klimchuk, J. A., Antiochos, S. K., & Mariska, J. T. 1987, ApJ, 320, 409

Klimchuk, J. A. & Gary, D. E. 1995, ApJ, 448, 925.

Lee, J., Hurford, G. J., & Gary, D. E. 1993, Sol. Phys., 144, 45

Lee, J., Gary, D. E., Hurford, G. J., & Zirin, H. 1993, in *The Magnetic and Velocity Fields of Solar Active Regions*, ed. H. Zirin, G. Ai, & H. Wang, A.S.P. Conf. Series 46, 287

Lee, J., McClymont, A. N., Mikić, Z., White, S. M., & Kundu, M. R. 1998a, ApJ, 501, in press

Lee, J., White, S. M., Kundu, M. R., Mikić, Z., & McClymont, A. N. 1998b, Sol. Phys., in press

Lee, J., White, S. M., Gopalswamy, N., & Kundu, M. R. 1997, Sol. Phys., 174, 175

McClymont, A. N., Jiao, L., & Mikić, Z. 1997, Sol. Phys., 174, 191

McClymont, A. N., & Mikić, Z. 1994, ApJ, 422, 899

Mikić, Z. & McClymont, A. N. 1994, in *Solar Active region Evolution: Comparing Models with Observations*, ed. K. S. Balasubramaniam & G. Simon, A.S.P. Conf. Series, 68, 225

Neupert, W. M. et al. 1997, BAAS, SPD meeting # 29, No. 01.15

Nindos, A., Alissandrakis, C. E., Gelfreikh, G. B., Kundu, M. R., Korzhavin, A. N., & Bogod, V. M. 1996, Sol. Phys., 166, 55

Nitta, N., White, S. M., Kundu, M. R., Gopalswamy, N., Holman, G. D., Brosius, J. W., Schmelz, J. T., Saba, J. L. R., & Strong, K. T. 1991, ApJ, 374, 374

Pallavicini, R. et al. 1981, ApJ, 247, 692

Rosner, R., Tucker, W. H., & Vaiana, G. S. 1978, ApJ, 220, 643

Schmahl, E. J., Kundu, M. R., Strong, K. T., Bentley, R. D., Smith, J. B., & Krall, J. R. 1982, Sol. Phys., 80, 233

Schmelz, J. T., Holman, G. D., Brosius, J. W., & Gonzalez, R. D. 1992, ApJ, 399, 733

Schmelz, J. T., Holman, G. D., Brosius, J. W., & Wilson, R. F. 1995, ApJ, 434, 786

Serio, S. et al. 1981, ApJ, 243, 288

Vesecky, J. F., Antiochos, S. K., & Underwood, J. H. 1979, ApJ, 233, 987

Vourlidas, A., Bastian, T. S., & Aschwanden, M. J. 1997, ApJ, 489, 403

White, S. M. & Kundu, M. R. 1997, Sol. Phys., 174, 31

Zheleznyakov, V. V. 1962, Soviet Astron., 6, 3

Zlotnik, E. Ya. 1968a, Soviet Astron., 12, 245

Zlotnik, E. Ya. 1968b, Soviet Astron., 12, 464

This preprint was prepared with the AAS LaTeX macros v4.0.

Fig. 1.— Ths figure illustrates the proposed method. The two surfaces shown are (simplified) hypothetical emission layers for 4.9 and 8.4 GHz, respectively, and the greyscale images on the surfaces are the actual observed X mode microwave images of AR 6615. The coordinates (x, y) form the sky plane, while z is the line of sight. Several magnetic field lines connecting the two emission layers are shown. Magnetic field lines numbered 1–3 should connect regions of similar temperatures on the two layers if they are correctly predicted by the photospheric field extrapolation. But there can be field lines such as line 4 that do not pass both but only one layer.

Fig. 2.— White contours outline regions inside of which the corona is optically thick ($\tau_n \geq 1$) due to gyroresonant opacity at $n = 3$ and $n = 4$ in the X and O modes (left and right panels, respectively) at 4.9 and 8.4 GHz (upper and lower panels, respectively). The background greyscale images are the observed radio intensity maps in LC and RC polarization states (left and right panels, respectively) at the corresponding frequencies; here the darker greys indicate brighter emission.

Fig. 3.— The left panels show contours of the X-mode 4.9 GHz image plotted on a greyscale presentation of the 8.4 GHz, together with a grid of points on each layer. Black plus symbols are starting points for field line trasing on the 4.9 GHz emission later and white symbols are the ending points on the 8.4 GHz emission layer. The white plus symbols right underneath the black plus symbols are those connected by the line of sight (LOS); the white plus and diamond symbols are those connected by potential field lines and nonlinear force–free field lines, respectively. In this part of the active region magnetic fields are nearly potential and both the PF and the FFF predict similar results. To the right of each image, the corresponding scatter plot of brightness temperature at 4.9 GHz versus that at 8.4 GHz for the connected points is shown together with linear correlation, r.

Fig. 4.— Same as Figure 3 but in the highly sheared area of AR 6615. The left panels show contours of the X-mode 4.9 GHz image plotted on a greyscale presentation of the 8.4 GHz, together with a grid of points on each layer (black plus symbols: 4.9 GHz; white plus symbols: 8.4 GHz) which are connected by the line of sight in the upper panel, by potential field lines in the middle panel, and by nonlinear force–free field lines in the bottom panel.

Fig. 5.— This plot reproduces Figure 4 but for the O mode, and with the addition of the bottom row of panels. In the upper three rows the O mode emission is assumed to be optically thick in the $n = 4$ harmonic layer. In the bottom panel we show the effect of assuming that the 8.4 GHz O mode emission arises on the $n = 3$ harmonic layer while the 4.9 GHz emission still comes from the $n = 4$ layer. In the bottom left panel, the black plus symbols again mark the field line intersections with the $n = 4$ 4.9 GHz layer, while

the white cross symbols are the corresponding 8.4 GHz points in the $n = 3$ layer in the PF model and the white squares are the corresponding 8.4 GHz points in the $n = 3$ layer in the FFF model.

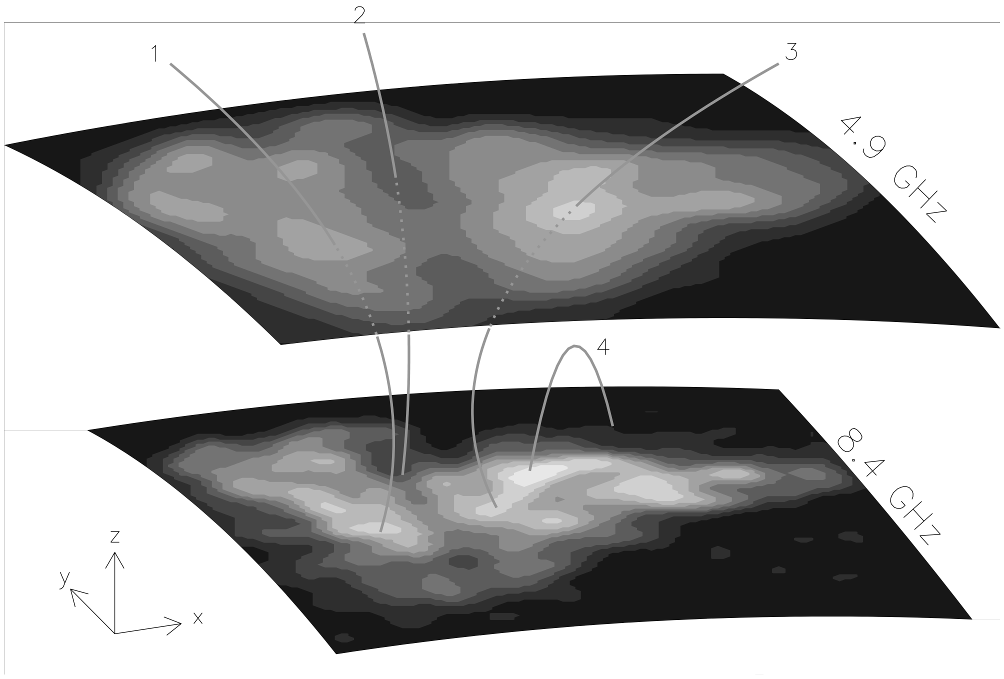
1
2
3
4
4.9 GHz
8.4 GHz
z
y
x

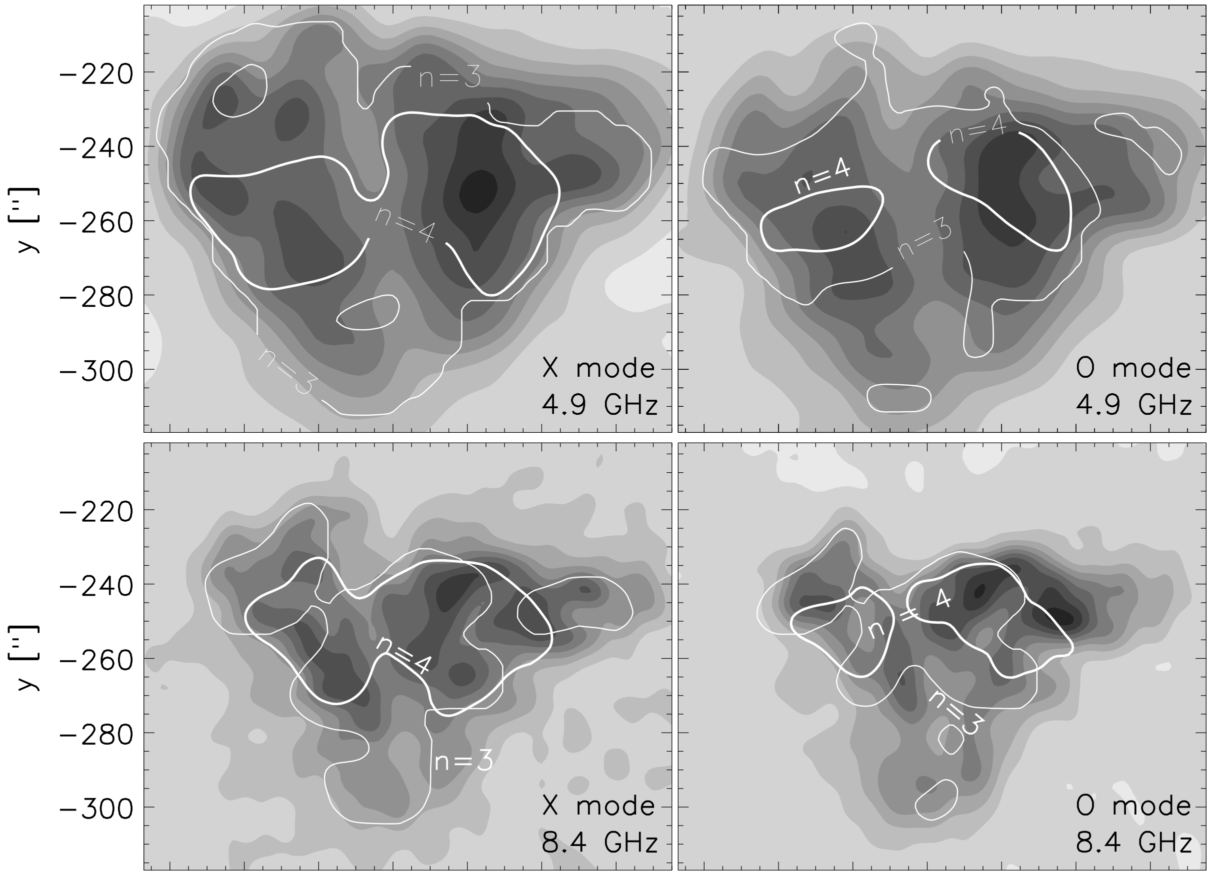
−220
−240
−260
−280
−300
y ['']
n=3
n=4
n=3
X mode
4.9 GHz
n=4
n=4
n=3
O mode
4.9 GHz
n=4
n=3
X mode
8.4 GHz
n=4
n=3
O mode
8.4 GHz
360 380 400 420 440 460 480
x ['']

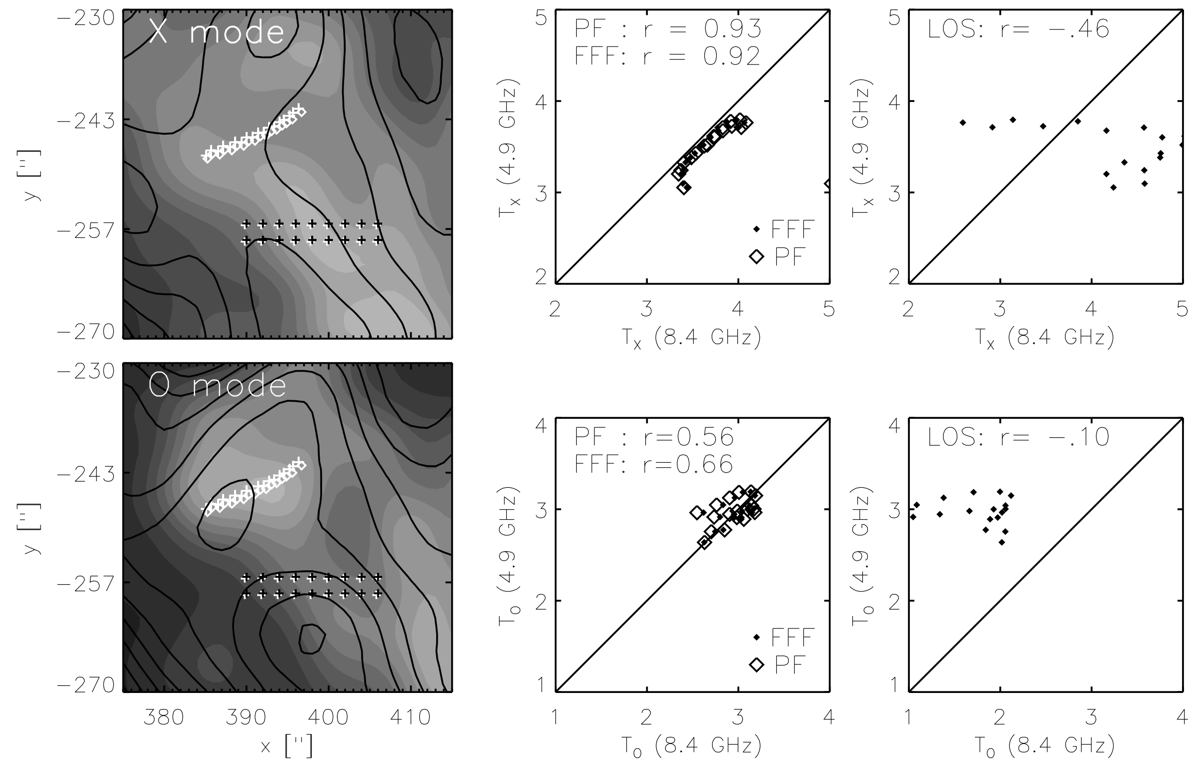
X mode
O mode
y ['']
x ['']
PF : r = 0.93
FFF: r = 0.92
FFF
PF
LOS: r= −.46
T_x (4.9 GHz)
T_x (8.4 GHz)
PF : r=0.56
FFF: r=0.66
LOS: r= −.10
T_o (4.9 GHz)
T_o (8.4 GHz)

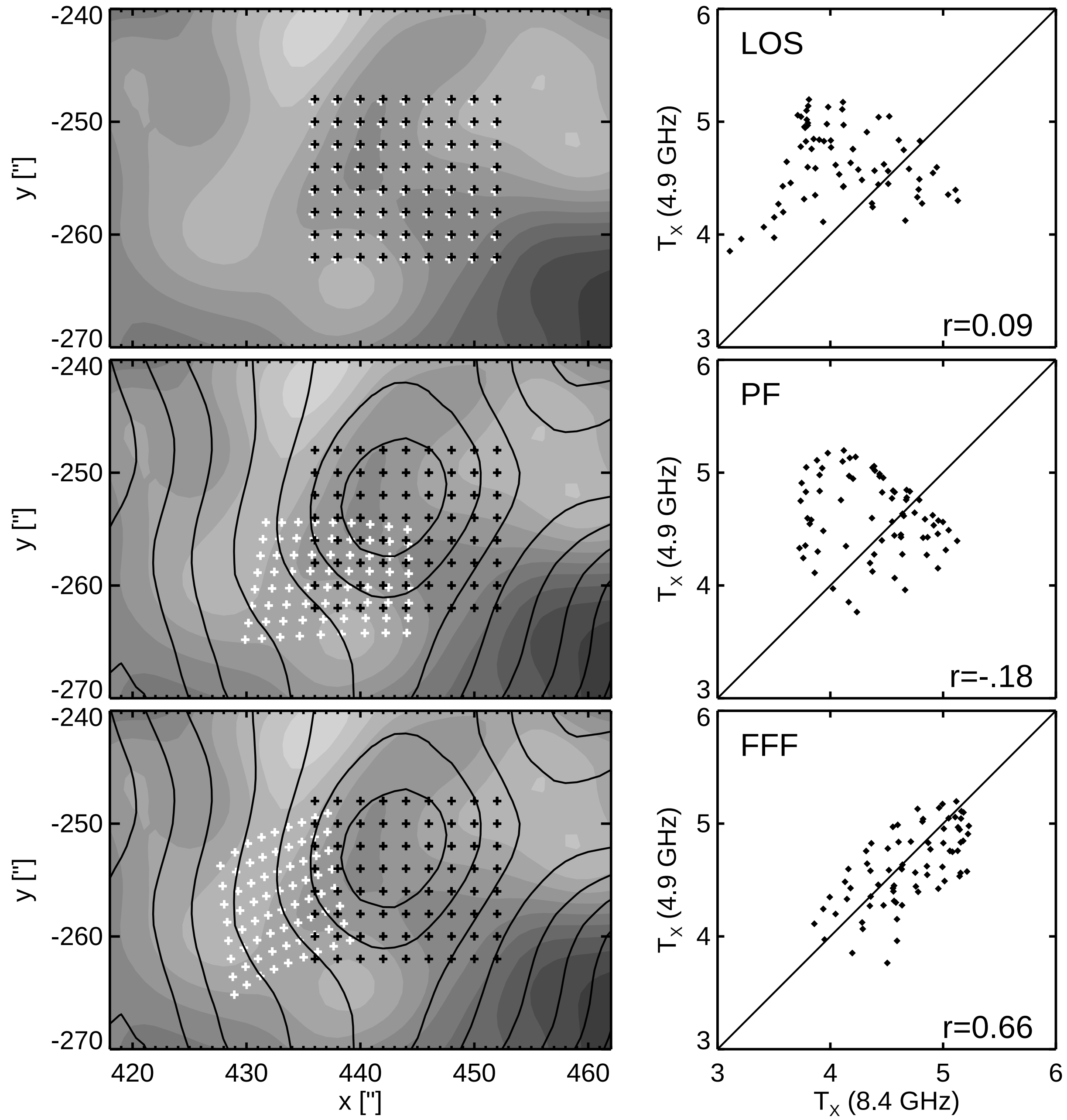

LOS
r=0.09
PF
r=-.18
FFF
r=0.66
y ['']
x ['']
T_X (4.9 GHz)
T_X (8.4 GHz)
-240
-250
-260
-270
420
430
440
450
460
3
4
5
6

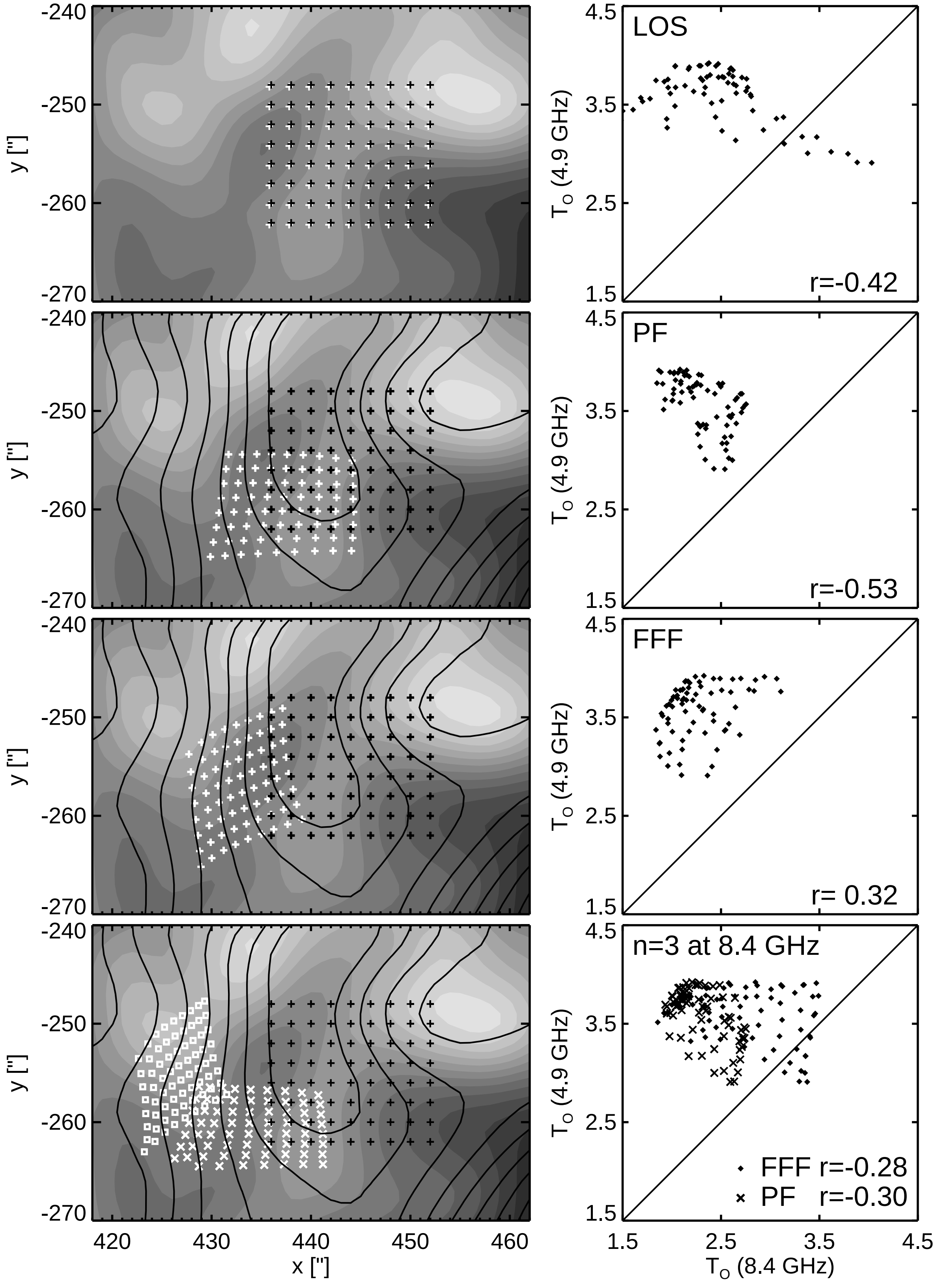

LOS
r=-0.42
PF
r=-0.53
FFF
r= 0.32
n=3 at 8.4 GHz
FFF r=-0.28
PF r=-0.30
y ["]
x ["]
T_O (4.9 GHz)
T_O (8.4 GHz)